치의학박사 학위논문

Differentiation between chondrosarcoma and synovial chondromatosis of the temporomandibular joint using computed tomography and magnetic resonance imaging

CT와 MR 영상을 이용한

측두하악관절 연골육종과 활액연골종증의 감별

2021년 2월

서울대학교 대학원

치의과학과 영상치의학 전공

장 봉 근

Differentiation between chondrosarcoma and synovial chondromatosis of the temporomandibular joint using computed tomography and magnetic resonance imaging

지도교수 허 경 회

이 논문을 치의학박사 학위논문으로 제출함
2020년 10월

서울대학교 대학원
치의과학과 영상치의학 전공
장 봉 근

장봉근의 박사 학위논문을 인준함
2021년 1월

위 원 장 허 민 석 (인)
부 위 원 장 허 경 회 (인)
위 원 이 상 훈 (인)
위 원 윤 혜 정 (인)
위 원 염 한 결 (인)

Abstract

Differentiation between chondrosarcoma and synovial chondromatosis of the temporomandibular joint using computed tomography and magnetic resonance imaging

Bong-Geun Jang, D.D.S.

Department of Oral and Maxillofacial Radiology,

Graduate School, Seoul National University

(Directed by Prof. Kyung-Hoe Huh, DDS, MSD, PhD)

Objectives

Chondrosarcoma (CS) and synovial chondromatosis (SC) are representative tumors of the temporomandibular joint (TMJ), producing cartilaginous calcification within the mass and causing bone changes of the mandibular condyle and/or articular eminence/glenoid fossa. Differentiating between CS and SC is essential because they require different therapeutic approaches. Clinicians, radiologists, and pathologists have difficulties in the differentiation

of CS and SC of the TMJ. The aim of this study is to identify CT and MR features to differentiate CS from SC of the TMJ.

Materials and Methods

CT and MRI scans of twelve and thirty-five patients with histopathologically confirmed CS and primary SC of the TMJ were retrospectively reviewed. Imaging features including the lesion epicenter, destruction/sclerosis of the mandibular condyle, destruction/sclerosis of the articular eminence/glenoid fossa, infiltration into the tendon of the lateral pterygoid muscle (LPM), pattern of calcification, periosteal reaction, osteophyte, peripheral enhancement, internal enhancement, and mean lesion size were assessed by two oral and maxillofacial radiologists.

Interobserver agreement for each imaging variables was assessed by calculation of Cohen's kappa coefficient for qualitative variables and intraclass correlation coefficient (ICC) for quantitative variables.

High-risk clinical or imaging features were defined as features that were significantly more frequent in CS than in SC based on statistics such as Fisher's exact test, chi-square test, linear-by-linear association test, Student's t-test, and receiver operating characteristic (ROC) analysis. In the first step, a comparison on clinical or imaging variables between CS and SC was performed with Fisher's exact test, chi-square test, or linear-by-linear association test for qualitative variables and with Student's t-test for

quantitative variables. In the second step, for each clinical or imaging variables which was significant through the first step, ROC analysis with the determination of Youden index was performed to identify the best cut–off value in order to differentiate between the two diseases. For statistically significant variables through the first step, the high-risk clinical or imaging features were finally determined based on the cut-off value. To figure out the diagnostic performance of each high-risk clinical or imaging features, sensitivity, specificity, accuracy, positive predictive value (PPV), negative predictive value (NPV), and area under the ROC curve (AUC) for differentiation were calculated by using the best cut-off values. Based on the cut–off values, a point of 1 or 0 was given. The point "1" indicates high–risk clinical or imaging feature for CS, while the point "0" indicates SC. A composite score for differentiating CS from SC was created by summing those points from each variables. Diagnostic performances predicting CS using composite scores were evaluated again using ROC analysis.

Results

Imaging variables, which were significant by Fisher's exact test, linear-by-linear association test, or Student's t-test, were as follows: 1) lesion epicenter, 2) destruction of the mandibular condyle, 3) destruction of the articular eminence/glenoid fossa, 4) sclerosis of the articular eminence/glenoid fossa, 5) infiltration into the tendon of the LPM, 6) calcification pattern, 7) periosteal reaction, 8) internal enhancement, and 9) mean lesion size.

The cut-off values for each statistically significant variables to differentiate CS from SC were as follows; 1) ‘Mandibular condyle’ for lesion epicenter, 2) ‘Presence’ for destruction of the mandibular condyle, 3) ‘Absence’ for destruction of the articular eminence/glenoid fossa, 4) ‘Absence’ for sclerosis of the articular eminence/glenoid fossa, 5) ‘Presence’ for infiltration into the tendon of LPM, 6) ‘Stippled calcification’ for pattern of calcification, 7) ‘Presence’ for periosteal reaction, 8) ‘Presence’ for internal enhancement, and 9) ‘30.5 mm’ for lesion size.

High-risk imaging features were as follows; 1) ‘Mandibular condyle’ for lesion epicenter, 2) ‘Presence’ for destruction of the mandibular condyle, 3) ‘Absence’ for destruction of the articular eminence/glenoid fossa, 4) ‘Absence’ for sclerosis of the articular eminence/glenoid fossa, 5) ‘Presence’ for infiltration into the tendon of LPM, 6) ‘Stippled calcification’ or ‘Absence of calcification’ for pattern of calcification, 7) ‘Presence’ for periosteal reaction, 8) ‘Presence’ for internal enhancement, and 9) ‘≥30.5 mm’ for lesion size.

For each high-risk imaging features, the maximum value of sensitivity (100%) was shown in presence of infiltration into the tendon of the LPM and internal enhancement, while the maximum value of specificity (100%) was revealed in lesion epicenter at the mandibular condyle. The highest value of AUC (0.929 [95% CI, 0.855–1.000]) was shown in infiltration into the tendon of the LPM. The best cut-off value of composite scoring model to discriminate CS from SC was +4 points, with the area under the curve of 0.958 [95% CI, 0.864–1.000].

Conclusion

CT and MRI show outstanding performance of AUC (0.958 [95% CI, 0.864–1.000]) in differential diagnosis between CS and SC.

Key Words: Chondrosarcoma, Synovial chondromatosis, Temporomandibular joint, Differential diagnosis, Imaging feature

Student number: 2018-37587

CONTENTS

LIST OF TABLES

LIST OF FIGURES

ABBREVIATION

SC	Synovial chondromatosis
CS	Chondrosarcoma
TMJ	Temporomandibular joint

INTRODUCTION

Chondrosarcoma (CS) and synovial chondromatosis (SC) are representative tumors of the temporomandibular joint (TMJ), producing cartilaginous calcification within the mass and causing bone changes of the mandibular condyle and/or articular eminence/glenoid fossa[1-6]. CS is a malignant neoplasm generating cartilage matrix in which calcification can occur[6,7] and accounts for about 20–27% of all primary malignant bone tumors of the whole body[6,8]. SC is a benign neoplasm forming nodular cartilage in synovial joints[1,2]. The cartilaginous nodules may detach from the synovium and produce intra-articular loose bodies[3]. Those cartilaginous loose bodies are nourished by synovial fluid and can be calcified[5]. The patients suffering from CS or SC usually presents with pain, trismus and/or swelling[2,4].

Differentiating between CS and SC is essential because they require different therapeutic approaches. The gold standard for CS treatment is surgical resection[9]. Among prognostic factors such as the extent of surgical resection, grade, and TNM classification, a wide local resectability is the most important[10]. Resection for CS must be as wide as possible, and a large healthy tissue margin of more than 2 cm seems to positively affect prognosis[9,11]. In contrast, the treatment of SC generally includes open joint surgery to remove all affected synovium and loose bodies, but usually saves the mandibular condyle. If the lesion cause destruction of the mandibular condyle, high condylectomy may be considered[12].

Clinicians, radiologists, and pathologists have difficulties in the differentiation of CS and SC of the TMJ[13-16]. Their presenting symptoms are similar and their imaging features have not been systematically compared in the previous studies. Because SC and low-grade CS share some overlapping histopathologic features such as binucleated chondrocytes and considerable cellularity, problems have been raised in differential histopathologic diagnosis[17-20]. Histopathological discrimination between CS and SC is more difficult in case of secondary CS, which develops from a pre-existing cartilaginous neoplasm such as SC, than in a case of primary CS, which arises de novo[13]. Thus, the differentiation between CS and SC based on imaging may be very important. Recently, imaging features of CS, such as outward growth from the mandibular condyle and infiltration into the tendon of lateral pterygoid muscle (LPM) attachment, were reported and the possibility of its differentiation from other benign tumors of the TMJ was suggested[4]. However, comparisons by using consistent imaging parameters for CS and SC of the TMJ have not been reported.

The aim of this study was to compare imaging parameters and to assess their diagnostic performance for differentiation of CS from SC of the TMJ, using CT and MR features.

MATERIALS AND METHODS

This retrospective study was approved by the institutional review board, and informed consent was waived.

Histopathologic database of our institute between January 2001 and October 2020 was searched for patients who were finally diagnosed with CS and SC of the TMJ. For SC, patients with secondary SC, caused by degenerative change, were excluded and only those with primary SC were included. Twelve and thirty-five patients were identified for CS and SC, respectively.

Clinical records were obtained from electronic medical records. Demographic characteristics, side (right or left), and chief complaint (swelling, pain, or trismus) were analyzed.

Image Acquisition

For all CS patients, both multidetector computed tomography (MDCT) and magnetic resonance imaging (MRI) were performed. MDCT with contrast media was performed on eleven CS patients. MRI with contrast media was undertook on all CS patients.

For SC patients, MDCT was performed on twenty-seven patients, cone beam CT (CBCT) on thirteen patients, and MRI on twenty-four patients. All SC patients underwent either MDCT or MRI examination for soft tissue evaluation, and MDCT or CBCT examination for hard tissue evaluation. Twelve SC patients undertook either MDCT and/or MRI examination, with

contrast media.

MDCT examination

MDCT imaging with contrast media was performed on eighteen patients of forty-seven patients using a MDCT scanner (Sensation 10; Siemens Healthcare, Erlangen, Germany) from the orbit to the bottom of the sternum. The scan parameters used were 120 kV, 150 mAs, and 1–2 mm slice collimation. After scanning the scout image, contrast media (1.5 cc/kg, iopromide, Ultravist 370; Bayer Healthcare, Berlin, Germany) was injected intravenously at a flow rate of 2–3 ml/s. MDCT imaging without contrast media was obtained on twenty-one patients of forty-seven patients

MR examination

A 3.0 T MR system (Skyra; Siemens Healthcare, Erlangen, Germany) was used on twenty patients of forty-seven patients, and a 1.5 T MRI system (Signa HDxt; GE Medical Systems, Milwaukee, WI, USA) was used in sixteen patients of forty-seven patients. A 32-channel and a 16-channel phased-array coil were used for the 3.0 and 1.5 T scanners, respectively. A slice thickness of 4–6 mm, a matrix size of 320 × 240 or 320 × 192, and a field of view 22 × 22 or 19 × 19 cm were adapted. Axial, coronal, and sagittal non-fat-suppressed or fat-suppressed T2-weighted fast spin echo [repetition time (TR): 3,000–5,600 ms; echo time (TE): 60–110 ms]; sagittal proton-density fast spin echo (TR: 2600–2700 ms; TE: 15–20 ms); axial and coronal

non-fat-suppressed T1-weighted spin echo (TR: 500–600 ms; TE: 10–15 ms); axial, coronal, and sagittal gadolinium-enhanced fat-suppressed T1-weighted spin echo (TR: 500–700 ms; TE: 9–15 ms) were acquired. MRI with contrast media was performed on nineteen patients of forty-seven patients. Contrast media (0.1 mmol/kg, gadopentetate dimeglumine, Magnevist; Schering AG, Berlin, Germany) was injected intravenously at a flow rate of 1.5 ml/s. MRI without contrast media was performed on seventeen patients of forty-seven patients

CBCT examination

CBCT imaging was performed by using a DINNOVA3 (HDXWILL, Seoul, Korea), with field of view of 20 × 19 cm for men and 20 × 14 cm for women, 100 kVp, 9 mAs, and isotropic voxels of 0.3 mm.

Analysis of Imaging Features

Imaging features assessed were lesion epicenter, destruction or sclerosis of the mandibular condyle or articular eminence/glenoid fossa, infiltration into the tendon of the LPM in the pterygoid fovea, calcification, periosteal reaction, osteophyte, enhancement pattern, and lesion size. Each imaging feature was reviewed through a multiplanar assessment of axial, coronal, and sagittal images.

The lesion epicenter was assessed as mandibular condyle or joint space on MR and/or MDCT images. The presence of bone destruction or sclerosis was

assessed on CBCT or MDCT images. The infiltration into the tendon of the LPM was defined as the replacement of the LPM attachment by the mass in the pterygoid fovea, and also assessed as presence or absence. According to World Health Organization classification scheme[21,22], the pattern of calcification was classified, on MDCT or CBCT images, as absence of calcification, stippled type (punctate) (Figs 1 and 2), flocculent type (irregularly shaped), ring-and-arc type (curvilinear, comma-shaped, or annular) with or without stippled and flocculent type (Figs 1 and 4), or popcorn type (amorphous calcifications often with ring-and-arc type) which is similar to popped corn kernels (Fig 1). The presence of periosteal reaction and osteophyte of the mandibular condyle was also assessed on MDCT or CBCT images. The presence of internal enhancement was evaluated only on contrast-enhanced MDCT or MR images. The lesion size on MR or MDCT images was quantitatively assessed as the longest diameter (X) on an axial plane, as the longest diameter (Y) perpendicular to the longest diameter on the axial plane, and as the longest diameter (Z) in craniocaudal direction on a coronal or sagittal plane. The lesion size was calculated by dividing the sum of X, Y, and Z by 3. To evaluate whether the lesion's shape is a long saddle, analogous to the shape of the synovium which is the origin of SC, or sphere, analogous to the shape of the mandibular condyle which is the origin of most of CS, the ratio of X to Z (X/Z) was calculated.

Two oral and maxillofacial radiologists with 20 and 15 years of experience, respectively, analyzed all CT and MRI scans for qualitative and quantitative

analyses, blinded to the histopathological and clinical information. In the cases of disagreement between the two radiologists, all discrepancies were resolved by consensus.

Statistical Analysis

Interobserver agreement for each imaging variable was assessed by calculation of Cohen's kappa coefficient for qualitative variables and intraclass correlation coefficient (ICC) for quantitative variables. The strength of Cohen's kappa coefficient was considered as follows: values less than 0.20, between 0.21 and 0.40, between 0.41 and 0.60, between 0.61 and 0.80, and greater than 0.81 are indicative of slight, fair, moderate, substantial, and almost perfect reliability, respectively[23]. The strength of ICC was considered as follows: values less than 0.5, between 0.5 and 0.75, between 0.75 and 0.9, and greater than 0.9 are indicative of poor, moderate, good, and excellent reliability, respectively[24].

High-risk clinical or imaging features were defined as features that were significantly more frequent in CS than in SC based on statistics such as Fisher's exact test, chi-square test, linear-by-linear association test, Student's t-test, and receiver operating characteristic (ROC) analysis. To find out high-risk clinical or imaging features, in the first step, comparisons of each clinical and imaging variables between CS and SC group were performed by Fisher's exact test, chi-square test, or linear-by-linear association test for qualitative variables and by Student's t-test for the quantitative variables with a .05

significance level. In the second step, for each clinical or imaging variables which was significant through the first step, ROC analysis with the determination of Youden index was performed to identify the best cut-off value in order to differentiate between the two diseases. For statistically significant variables through the first step, the high-risk clinical or imaging features were finally determined based on the cut-off value. To figure out the diagnostic performance of each high-risk clinical or imaging features, sensitivity, specificity, accuracy, positive predictive value (PPV), negative predictive value (NPV), and area under the ROC curve (AUC) for differentiation were calculated by using the best cut-off value. An AUC of 0.5 was considered as no discrimination, 0.5 to 0.7 as poor discrimination, 0.7 to 0.8 as acceptable, 0.8 to 0.9 as excellent, and higher than 0.9 as outstanding[25].

Finally, for each high-risk clinical or imaging variable, a score of 1 or 0 was assigned to each of them. The point “1” indicates a high-risk clinical or imaging feature for CS, while the point “0” indicates a favorable feature for SC. A composite scoring model for differentiating CS from SC was created by summing those points from each variable. ROC analysis was performed again to evaluate the best cut-off value of the composite scoring model to differentiate CS from SC.

IBM SPSS statistics 23 (SPSS Inc., Chicago, IL, USA) was used for statistical analysis. The values related to the sensitivity, specificity, accuracy, PPV, and NPV were calculated using Excel 2019 (Microsoft, Redmond, Wash,

USA).

.

Results

Analysis of Clinical Features

No statistically significant difference was found in age, male-to-female ratio, right-to-left ratio, or chief complaint such as swelling, pain, and trismus between CS and SC (Table 1).

Analysis of Imaging Features

All imaging features of CS and SC are summarized in Table 2. The interobserver agreement between the two readers was almost perfect and excellent for qualitative and quantitative variables, respectively ($P < .001$).

Imaging features, which were significant by Fisher's exact test, linear-by-linear association test, or Student's t-test, were as follows: 1) lesion epicenter ($P < .001$), 2) destruction of the mandibular condyle ($P = .037$), 3) destruction of the articular eminence/glenoid fossa ($P = .012$), 4) sclerosis of the articular eminence/glenoid fossa ($P < .001$), 5) infiltration into the tendon of LPM ($P < .001$), 6) pattern of calcification ($P = .008$), 7) periosteal reaction ($P = .001$), 8) internal enhancement ($P < .001$), 9) lesion size ($P < .001$). X, Y, and Z as well as lesion size (average of X, Y, and Z) were also significantly larger in CS by Student's t-test ($P < .001$). Presence or absence of calcification showed no statistical significance by Fisher's exact test ($P = .251$). However, when calcification pattern was considered as a dimensional continuum from absence of calcification to popcorn calcification, a tendency that calcification

disappeared was observed in CS by linear-by-linear association test (P = .008).

Diagnostic Performance of Each High-risk Imaging Features and Composite Scoring Model

The cut-off values for each statistically significant variable to differentiate CS from SC were as follows; 1) 'Mandibular condyle' for lesion epicenter, 2) 'Presence' for destruction of the mandibular condyle, 3) 'Absence' for destruction of the articular eminence/glenoid fossa, 4) 'Absence' for sclerosis of the articular eminence/glenoid fossa, 5) 'Presence' for infiltration into the tendon of LPM, 6) 'Stippled calcification' for pattern of calcification, 7) 'Presence' for periosteal reaction, 8) 'Presence' for internal enhancement, and 9) '30.5 mm' for lesion size (Fig 4).

High-risk imaging features for differentiating CS from SC were as follows; 1) 'Mandibular condyle' for lesion epicenter, 2) 'Presence' for destruction of the mandibular condyle, 3) 'Absence' for destruction of the articular eminence/glenoid fossa, 4) 'Absence' for sclerosis of the articular eminence/glenoid fossa, 5) 'Presence' for infiltration into the tendon of LPM, 6) 'Stippled calcification' or 'Absence of calcification' for pattern of calcification, 7) 'Presence' for periosteal reaction, 8) 'Presence' for internal enhancement, and 9) '≥30.5 mm' for lesion size.

For differentiating CS from SC, sensitivity, specificity, accuracy, PPV, NPV, and AUC of each high-risk imaging features are listed in Table 3. The maximum value of sensitivity (100%) was obtained for infiltration into the

tendon of LPM and internal enhancement, while the maximum value of specificity (100%) was revealed for lesion epicenter. The single high-risk imaging feature that showed outstanding performance (AUC = 0.929 [95% CI, 0.855–1.000]) was infiltration into the tendon of LPM.

ROC analysis, performed on the 9-scale composite scoring model from the high-risk imaging features for CS, is presented in figure 5. The best cut-off value to distinguish CS from SC was observed for the presence of ≥4 high-risk imaging features (Youden index = 0.917, AUC = 0.958 [95% CI, 0.864–1.000]). This cut-off value showed 100.0%, 91.7%, 95.8%, 92.3%, and 100.0% values for sensitivity, specificity, accuracy, PPV, and NPV, respectively.

Table 1: Analysis of clinical features of chondrosarcoma and synovial chondromatosis

Independent variables	Total (47)			p-Value
		CS (12)	SC (35)	
Age[a]	49.3 ± 13.5	50.3 ± 15.6	48.9 ± 13.2	0.756
Sex[b]				0.659
Male	7 (14.9%)	1 (8.3%)	6 (17.1%)	
Female	40 (85.1%)	11 (91.7%)	29 (82.9%)	
Side[c]				0.679
Right	25 (53.2%)	7 (58.3%)	18 (51.4%)	
Left	22 (46.8%)	5 (41.7%)	17 (48.6%)	
Chief complaint				
Swelling[c]	11 (23.4%)	5 (41.7%)	6 (17.1%)	0.118
Pain[b]	43 (91.5%)	11 (91.7%)	32 (91.4%)	1.000
Trismus[b]	20 (42.6%)	8 (66.7%)	12 (34.3%)	0.089

[a]: Student's t-test, [b]: Fisher's exact test, [c]: chi-square test

Table 2: Analysis of imaging features for chondrosarcoma and synovial chondromatosis

Independent variables	Total [47]			p-Value	Interobserver agreement
		CS [12]	SC [35]		
Lesion epicenter[a,*]				<.001	.832[d]
Joint space	40 (85.1%)	5 (41.7%)	35 (100%)		
Mandibular condyle	7 (14.9%)	7 (58.3%)	0 (0%)		
Destruction of the mandibular condyle[a,*]	31 (66.0%)	11 (91.7%)	20 (57.1%)	.037	.905[d]
Sclerosis of the mandibular condyle[a]	23 (48.9%)	8 (66.7%)	15 (42.9%)	.193	.872[d]
Destruction of the articular eminence/glenoid fossa[a,*]	31 (66.0%)	4 (33.3%)	27 (77.1%)	.012	.856[d]
Sclerosis of the articular eminence/glenoid fossa[a,*]	29 (61.7%)	2 (16.7%)	27 (77.1%)	<.001	.861[d]
Infiltration into the tendon of lateral pterygoid muscle[a,*]	17 (36.2%)	12 (100.0%)	5 (14.3%)	<.001	.908[d]
Calcification[a]	37 (78.7%)	8 (66.7%)	29 (82.9%)	.251	.828[d]
Pattern of calcification[b,*]				.008	.835[d]
Absence	10 (21.3%)	4 (33.3%)	6 (17.1%)		
Stippled	9 (19.1%)	6 (50.0%)	3 (8.6%)		
Flocculent	4 (8.5%)	0 (0.0%)	4 (11.4%)		
Ring-and-arc	9 (19.1%)	0 (0.0%)	9 (25.7%)		
Popcorn	15 (31.9%)	2 (16.7%)	13 (37.1%)		
Periosteal reaction[a,*]	12 (25.5%)	8 (66.7%)	4 (11.4%)	.001	.827[d]
Osteophyte[a]	10 (21.3%)	2 (16.7%)	8 (22.9%)	1.000	.873[d]
Peripheral enhancement[a]	19 (79.2%)	11 (91.7%)	8 (66.7%)	.317	.864[d]
Internal enhancement[a,*]	15 (62.5%)	12 (100.0%)	3 (25.0%)	<.001	.830[d]
Lesion size[c,*]	28.5 ± 7.4	37.1 ± 8.2	25.6 ± 4.2	<.001	.932[e]
X/Z ratio[c]	1.6 ± 0.3	1.5 ± 0.2	1.7 ± 0.3	.067	.928[e]

LPM: lateral pterygoid muscle, [a]: Fisher's exact test, [b]: linear-by-linear association test, [c]: Student's t-test, [*]: statistically significant. [d]: Cohen's kappa coefficient, [e]: intraclass correlation coefficient, The values of lesion size and X/Z ratio were expressed as mean ± standard deviation.

Table 3: Diagnostic performance of each qualitative and quantitative parameter which showed a statistically significant difference for differentiating chondrosarcoma from synovial chondromatosis

	Prevalence	Sensitivity (%)	Specificity (%)	Accuracy (%)	PPV (%)	NPV (%)	AUC [95% CI]
Lesion epicenter (Mandibular condyle)*	CS 7/12 SC 0/35	58.3	100.0	89.4	100.0	87.5	0.792 [0.611–0.972]
Destruction of the mandibular condyle (Presence)*	CS 11/12 SC 20/35	91.7	42.9	55.3	35.5	93.8	0.673 [0.510–0.835]
Destruction of the articular eminence/glenoid fossa (Absence)*	CS 8/12 SC 8/35	66.7	77.1	74.5	50.0	87.1	0.719 [0.542–0.896]
Sclerosis of the articular eminence/glenoid fossa (Absence)*	CS 10/12 SC 8/35	83.3	77.1	78.7	55.6	93.1	0.802 [0.654–0.950]
Infiltration into the tendon of lateral pterygoid muscle (Presence)*	CS 12/12 SC 5/35	100.0	85.7	89.4	70.6	100.0	0.929 [0.855–1.000]
Calcification (Absence or stippled)*	CS 10/12 SC 9/35	83.3	74.3	76.6	52.6	92.9	0.729 [0.556–0.901]
Periosteal reaction (Presence)*	CS 8/12 SC 4/35	66.7	88.6	83.0	66.7	88.6	0.776 [0.604–0.948]
Internal enhancement (Presence)*	CS 12/12 SC 3/12	100.0	75.0	87.5	80.0	100.0	0.875 [0.719–1.000]
Mean lesion size (≥ 30.5 mm)*	CS 10/12 SC 5/35	83.3	85.7	85.1	66.7	93.8	0.889 [0.773–1.000]

*: The items in parentheses correspond to the characteristics of chondrosarcoma and a point of 1 was given if relevant imaging feature in the parentheses was present. PPV: positive predictive value, NPV: negative predictive value, AUC: area under the receiver operating characteristics

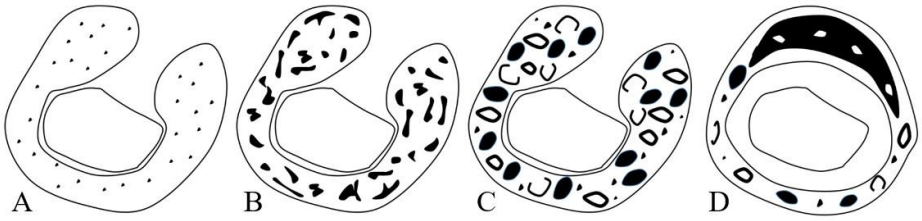

Figure 1 Schematic drawings of the four types of calcification patterns in the TMJ (A) stippled type, (B) flocculent type, (C) ring-and-arc type, and (D) popcorn type.

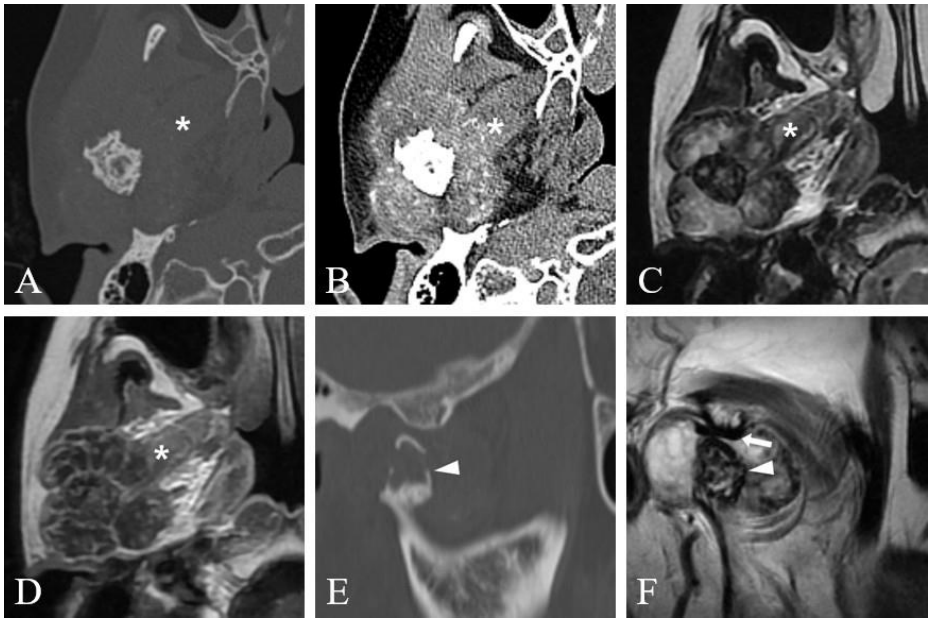

Figure 2 Representative images of chondrosarcoma of the right TMJ in a 54-year-old woman. (A–D) Axial MDCT, non-fat-suppressed T2-weighted MR, and contrast-enhanced T1-weighted MR images demonstrate a large mass infiltrating into the tendon of the lateral pterygoid muscle (asterisk) in the pterygoid fovea and showing septa-like internal enhancement. Stippled calcification and severely destroyed mandibular condyle with periosteal reaction are also revealed. (E and F) Sagittal MDCT and T2-weighted MR images present the mass epicenter of the mandibular condyle (arrow head). Note the disc (arrow) located between the destroyed mandibular condyle and the intact articular eminence.

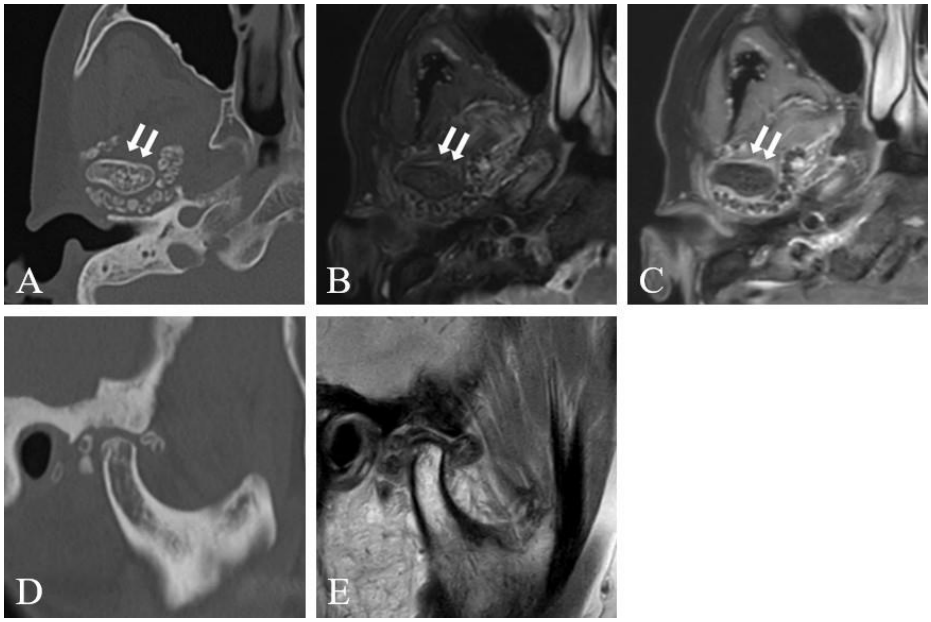

Figure 3 Representative images of synovial chondromatosis of the left TMJ in a 54-year-old woman. (A–C) Axial MDCT, fat-suppressed T2-weighted MR, and contrast-enhanced T1-weighted MR images show that the mass, containing ring-and-arc calcification, does not infiltrate into the tendon of lateral pterygoid muscle, but surrounds the muscle attachment (white arrows). (D and E) Sagittal MDCT and proton density-weighted MR image demonstrate the lesion epicenter of joint space. Note severe sclerosis of the articular eminence/glenoid fossa, but relatively intact bone marrow of the mandibular condyle.

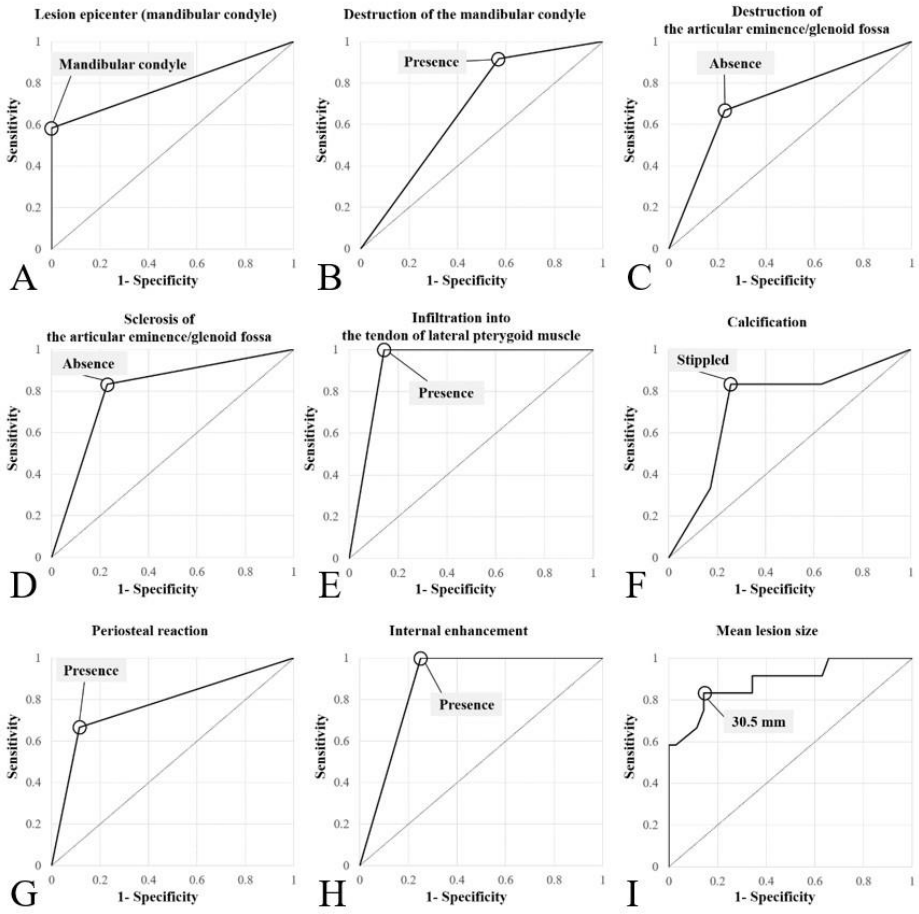

Figure 4 Receiver operating characteristic curve for qualitative and quantitative variables showed that the best cut-off values for differentiating chondrosarcoma from synovial chondromatosis were: (A) 'Mandibular condyle' for lesion epicenter (YI= 0.583, AUC = 0.792 [95% CI, 0.611–0.972]), (B) 'Presence' for destruction of the mandibular condyle (YI = 0.346, AUC = 0.673 [95% CI, 0.510–0.835]), (C) 'Absence' for destruction of the articular eminence/glenoid fossa (YI = 0.438, AUC = 0.719 [95% CI, 0.542–0.896]), (D) 'Absence' for sclerosis of the articular eminence/glenoid fossa (YI = 0.604, AUC = 0.802 [95% CI, 0.654–0.950]), (E) 'Presence' for infiltration into the tendon of lateral pterygoid muscle (YI = 0.857, AUC = 0.929 [95% CI, 0.855–1.000]), (F) 'Absence of calcification or stippled calcification' for pattern of calcification (YI = 0.576, AUC = 0.729 [95% CI, 0.556–0.901]), (G) 'Presence' for periosteal reaction (YI = 0.553, AUC = 0.776 [95% CI, 0.604–0.948]), (H) 'Presence' for internal enhancement (YI = 0.750, AUC = 0.875 [95% CI, 0.719–1.000]), and (I) '30.5 mm' for lesion size (YI = 0.690, AUC = 0.889 [95% CI, 0.773–1.000]). YI = Youden index, AUC = area under the receiver operating characteristic curve.

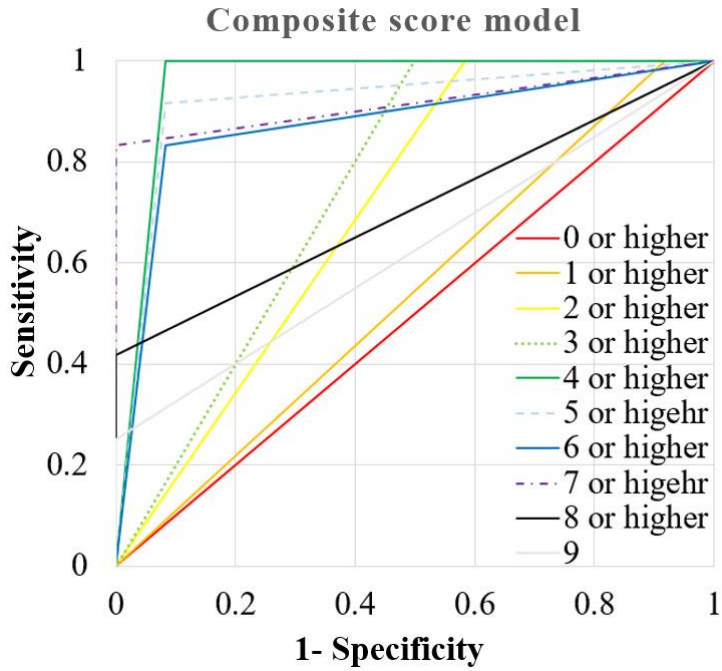

Figure 5 The receiver operating characteristic (ROC) curves of composite scores for distinguishing chondrosarcoma (CS) from synovial chondromatosis (SC). The score was assessed by giving 1 point for each of the following high-risk imaging features for chondrosarcoma: lesion epicenter of the mandibular condyle, destruction of the mandibular condyle, no destruction of the articular eminence/glenoid fossa, no sclerosis of the articular eminence/glenoid fossa, infiltration into the tendon of lateral pterygoid muscle, absence or stippled calcification, periosteal reaction, internal enhancement, and ≥ 30.5 mm for lesion size. The ROC curve of the composite score of ≥4 (dark green) has the highest AUC value of 0.958 [95% CI, 0.864–1.000], followed by the composite score of ≥5 and 7 (dashed bright blue and dashdotted purple, AUC value of 0.917 [95% CI, 0.786–1.000], respectively), composite score of ≥6 (dark blue, AUC value of 0.875 [95% CI, 0.719–1.000]), composite score of ≥3 (dotted green, AUC value of 0.750 [95% CI, 0.546–0.954]), composite score of ≥2 and 8 (yellow and black, AUC value of 0.708 [95% CI, 0.494–0.923]), composite score of 9 (gray, AUC value of 0.625 [95% CI, 0.397–0.853]), composite score of ≥1 (orange, AUC value of 0.542 [95% CI, 0.307–0.777]), and composite score of 0 (red, AUC value of 0.500 [95% CI, 0.264–0.736]).

Discussion

The present study investigated CT and MR imaging features to differentiate between CS and SC of the TMJ. The imaging distinction between the two diseases is very important because pre-operative histopathological examination such as fine needle aspiration biopsy, punch biopsy, or even incisional biopsy may yield low rate of correct differential diagnosis between CS and SC[4,13]. The present study demonstrated 9 imaging features to differentiate between CS and SC. The single imaging feature with the highest performance for the differential diagnosis was infiltration into the tendon of the LPM (AUC = 0.929 [95% CI, 0.855–1.000]), followed by lesion size (AUC = 0.889 [95% CI, 0.773–1.000]), internal enhancement (AUC = 0.875 [95% CI, 0.719–1.000]), and sclerosis of the articular eminence/glenoid fossa (AUC = 0.802 [95% CI, 0.654–0.950]). Moreover, with the combination of the 9 imaging features, the diagnostic performance of the 9-scale composite scoring model was significantly improved for differentiating CS from SC.

Infiltration into the tendon of the LPM demonstrated the highest AUC (0.929 [95% CI, 0.855–1.000]) and sensitivity (100%) for prediction of CS. Infiltration into the tendon of the LPM in CS was first reported in the previous study[4]. The lesion epicenter of the mandibular condyle and resultant infiltration into the tendon of the LPM in CS could be explained by the fact that most CSs are of the conventional intramedullary type[8]. While, all SCs in the present study showed lesion epicenter of the joint space, which could be

understood by the fact that the joint synovium is the origin of SCs[26]. The benign tumor arising in the synovium rarely infiltrated into the tendon of the LPM in the present study. This imaging feature of infiltration into the tendon of the LPM could be strong discriminator of CS from other benign tumors of the TMJ.

Lesion size of CS was significantly larger than that of SC, with cut-off value of ≥ 30.5 mm. According to the Milgram's classification of SC, which divided SC into onset phase I (intrasynovial involvement), transitional phase II (intrasynovial involvement and free bodies), and resolution phase III (multiple free bodies), onset phase I represents an inflammatory intrasynovial process with pain and swelling[26]. Additionally, movement of the mandibular condyle will exert further stimulus to the inflamed synovium, which might cause pain and discomfort in patients with SCs relatively in early stage. On the other hand, CSs, with malignant nature, can show more rapid growth and resultant larger size compared to SCs. In the whole body, CSs are large tumors, and most of them exceed 4 cm in maximal lesion size[8,27]. While, average lesion size of 25 cases of SCs of the whole body, including large joints such as shoulder, knee, and ankle, was 3.9 × 1.7 cm[28].

Presence of internal enhancement was significantly more frequent in CS than in SC, and showed high sensitivity (100%) for CS in the present study. Heterogeneous solid and focal solid internal enhancement in CS may represent malignant cells rather than cartilaginous tissue[4]. On the other hand, septa-like enhancement in cartilaginous tumors or cartilaginous tumor-like

conditions such as SC is thought to be fibrovascular tissue caused by a lobulated growth pattern and known to be more commonly located at the periphery of the tumors (Fig 2)[27-32]. Thus, various patterns of internal enhancement may allow differentiation of CS from other benign tumors.

Destruction of the mandibular condyle and no destruction/sclerosis of the articular eminence/glenoid fossa were significantly more commonly observed in CS than in SC, respectively. These significant differences could be explained by the fact that most of the CS have lesion epicenter of the mandibular condyle, while SC has lesion epicenter of the joint space, especially the superior joint space[33,34]. The articular disk may protect the articular eminence/glenoid fossa from the mass of CS which had epicenter at the mandibular condyle, and may protect the mandibular condyle from the mass of SC which had epicenter at the superior joint space.

Periosteal reaction was present significantly more frequent in CS compared to in SC in the present study. Periosteal reaction has previously been found to favor CS in femur, humerus, tibia, fibula, hands, and feet[35-38]. Periosteal reaction in SC of whole body has been rarely observed with 12% cases[28,29], which is constant with the present study. When discriminating between CS and enchondroma which has benign features like SC in whole body, periosteal reaction was significant imaging feature for CS[37], but it was not significant in another study[35]. Pattern of periosteal reaction, such as spiculate, parallel, or solid pattern, as well as presence of periosteal reaction, might play an important role in differentiating CSs from other benign tumors, and it needs

further study.

Absence of calcification and stippled calcification were significantly more observed in CS, while flocculent, ring-and-arc, and popcorn calcification were in SC in the present study. This result might be explained by the fact that coalescence of multiple loose bodies can occur in SC[5,30]. About 67% and more than 80% of the CS and SC patients in the present study had a prevalence of calcifications, which is consistent with the observations of previous research that showed 60–78% and 70–95% prevalence of calcifications in CS and SC of the whole body, respectively[5,8,29]. There were reports that identifying the pattern of calcification could not help in differentiating between benign and malignant chondroid tumors[27,35]. However, those reports did not apply the classification system of calcification according to World Health Organization classification scheme[21,22], which were used in the present study and it showed acceptable diagnostic performance (AUC = 0.729 [95% CI, 0.556–0.901]).

Eight out of nine imaging features showed outstanding, excellent, or acceptable diagnostic performance according to AUC. The 9-scale composite scoring model yielded even the most powerful diagnostic performance (AUC = 0.986 [95% CI, 0.950–1.000]). Imaging features of surrounding structures, such as LPM, mandibular condyle, and articular eminence/glenoid fossa, are not always reliable as those imaging features may mimic each other when CS occurs in the joint space or SC in inferior joint space (Figs 6 and 7). Patient in figure 6 was clinically misdiagnosed as SC by an oral and maxillofacial

surgeon with 20 years of experience during incisional biopsy based on CT and MR scans. Patient in figure 7 was radiologically misdiagnosed as CS by other hospital's oral and maxillofacial radiologists based on MR scans, and referred to our hospital. In the case of CS in joint space or SC in inferior joint space, imaging features of tumor size and internal structures, such as calcification and internal enhancement, might help in discrimination. In figure 6, the patient earned total score 4 from two imaging features of surrounding structures and two imaging features of internal structures. In figure 7, the patient earned total score 3 not from tumor size and internal structures but imaging features of surrounding structures.

The present study has some limitations. First, this was a retrospective study with a small number of patients. A prospective study with larger number of patients from multicenter hospitals to confirm imaging features of present study would validate our results in the future. Second, regression analysis was desired to determine which independent variables matter more and how those variables interact with each other. But, in the present study, the number of those variables was large and the number of patients was small. So, regression analysis was impossible, and equal one point was given for each independent variable without weight when creating the 9-scale composite scoring model. Instead, the relative importance of each variable was suggested by presenting AUC values for each independent variable through ROC.

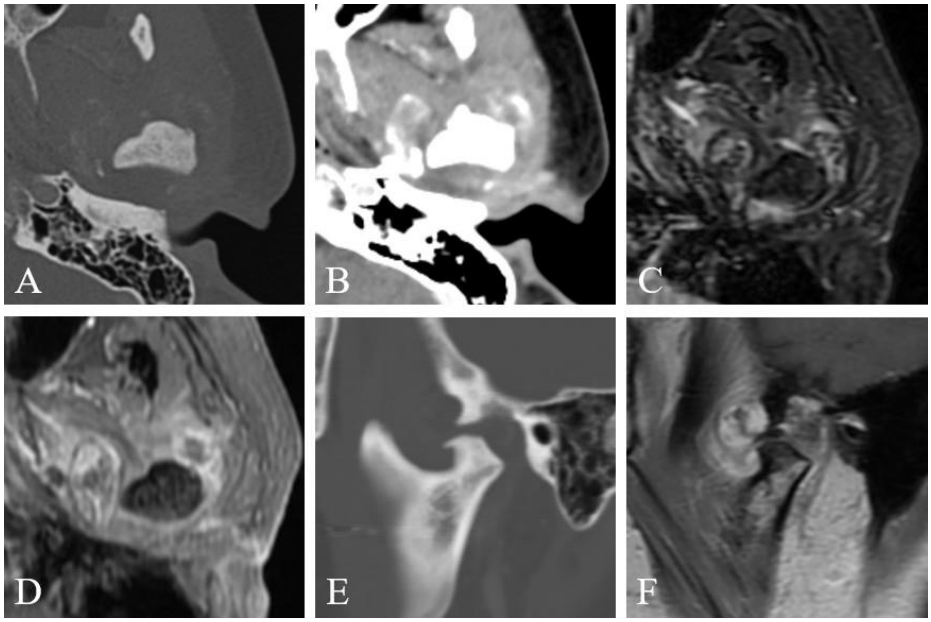

Figure 6 A 44-year-old woman complaining swelling and pain on the left TMJ and trismus. (A–D) Axial MDCT and fat-suppressed T2-weighted and contrast-enhanced T1-weighted MR images reveal a mass surrounding the mandibular condyle. (E and F) Sagittal MDCT and contrast-enhanced T1-weighted MR images demonstrate the mass epicenter of the joint space. Lesion epicenter of joint space, destruction and sclerosis of the articular eminence/glenoid fossa, absence of periosteal reaction and relatively small lesion size favor synovial chondromatosis. On the other hand, destruction of the mandibular condyle, infiltration into the tendon of lateral pterygoid muscle, stippled calcification, and internal enhancement favor chondrosarcoma. Histopathological examination after mass resection revealed the diagnosis of chondrosarcoma.

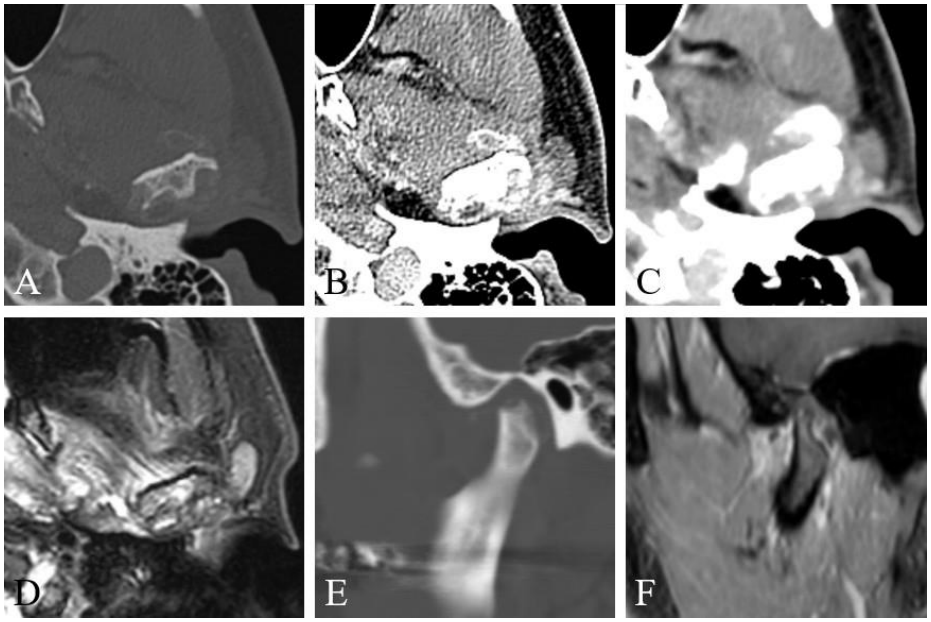

Figure 7 A 52-year-old man complaining pain on the left TMJ. (A–D) Axial MDCT and fat-suppressed T2-weighted MR images show a mass surrounding and destructing the mandibular condyle. (E and F) Sagittal MDCT and contrast-enhanced T1-weighted MR images reveal the mass epicenter of the joint space. Ring-and-arc calcification, intact tendon of the lateral pterygoid muscle in the pterygoid fovea, lesion epicenter of the joint space, and relatively small lesion size favor the imaging diagnosis of synovial chondromatosis. Result of a preoperative incisional biopsy was chondrosarcoma, but the final histopathological diagnosis was changed into synovial chondromatosis after mass resection.

CONCLUSION

CT and MR imaging features showed outstanding performance of AUC (0.958 [95% CI, 0.864–1.000]) in differential diagnosis between CS and SC, allowing selection of SC susceptible to mandibular condyle-sparing surgery, with the advantage of reducing post-surgical complications and improving the prognosis.

REFERENCES

1. Meng J, Guo C, Yi B, et al. **Clinical and radiologic findings of synovial chondromatosis affecting the temporomandibular joint.** *Oral Surg Oral Med Oral Pathol Oral Radiol Endod* 2010;109:441–8

2. von Lindern JJ, Theuerkauf I, Niederhagen B, et al. **Synovial chondromatosis of the temporomandibular joint: clinical, diagnostic, and histomorphologic findings.** *Oral Surg Oral Med Oral Pathol Oral Radiol Endod* 2002;94:31–8

3. Testaverde L, Perrone A, Caporali L, et al. **CT and MR findings in synovial chondromatosis of the temporo-mandibular joint: our experience and review of literature.** *Eur J Radiol*. 2011;78:414–8

4. Jang BG, Huh KH, Kang JH, et al. **Imaging features of chondrosarcoma of the temporomandibular joint: report of nine cases and literature review.** *Clin Radiol* 2020;75:878.e1–12

5. Murphey MD, Vidal JA, Fanburg-Smith JC, et al. **Imaging of synovial chondromatosis with radiologic-pathologic correlation.** *Radiographics* 2007;27:1465–88

6. Thorkildsen J, Taksdal I, Bjerkehagen B, et al. **Chondrosarcoma in Norway 1990–2013; an epidemiological and prognostic observational study of a complete national cohort.** *Acta Oncol* 2019;58:273–82

7. Ollivier L, Vanel D, Leclère J. **Imaging of chondrosarcomas.** *Cancer Imaging* 2003;4:36–8

8. Murphey MD, Walker EA, Wilson AJ, et al. **From the archives of the AFIP: imaging of primary chondrosarcoma: radiologic-pathologic correlation.** *Radiographics* 2003;23:1245–78

9. Slimani F, Iro MS, **Chondrosarcoma of the temporomandibular joint: A case report and review of the literature.** *EC Dental Science* 2019;1495–501

10. Lee SY, Lim YC, Song MH, et al. **Chondrosarcoma of the head and neck.** *Yonsei Med J* 2005;46:228–32

11. Mostafapour SP, Futran ND. **Tumors and tumorous masses presenting as temporomandibular joint syndrome.** *Otolaryngol Head Neck Surg* 2000;123:459–64

12. Huh JK, Park JY, Lee S, et al. **Synovial chondromatosis of the temporomandibular joint with condylar extension.** *Oral Surg Oral Med Oral Pathol Oral Radiol Endod* 2006;101:e83–8

13. Coleman H, Chandraratnam E, Morgan G, et al. **Synovialial chondrosarcoma arising in synovial chondromatosis of the temporomandibular joint.** *Head Neck Pathol* 2013;7:304–9

14. Ye ZX, Yang C, Chen MJ, et al. **Digital resection and reconstruction of TMJ synovial chondrosarcoma involving the skull base: report of a case.** *Int J Clin Exp Med* 2015;8:11589–93

15. Merrill RG, Yih WY, Shamloo J. **Synovial chondrosarcoma of the temporomandibular joint: a case report.** *J Oral Maxillofac Surg* 1997;55:1312–6

16. Ichikawa T, Miyauchi M, Nikai H, et al. **Synovial chondrosarcoma arising in the temporomandibular joint.** *J Oral Maxillofac Surg* 1998;56:890–4

17. Morris MR, Clark SK, Porter BA, et al. **Chondrosarcoma of the temporomandibular joint: case report.** *Head Neck Surg* 1987;10:113–7

18. Warner BF, Luna MA, Robert Newland T. **Temporomandibular joint neoplasms and pseudotumors.** *Adv Anat Pathol* 2000;7:365–81

19. Angiero F, Vinci R, Sidoni A, et al. **Mesenchymal chondrosarcoma of the left coronoid process: report of a unique case with clinical, histopathologic, and immunohistochemical findings, and a review of the literature.** *Quintessence Int* 2007;38:349–55

20. Oliveira RC, Marques KD, Mendonça AR, et al. **Chondrosarcoma of the temporomandibular joint: a case report in a child.** J Orofac Pain 2009;23:275–81

21. Davies AM, Pettersson H. **The WHO manual of diagnostic imaging:**

radiographic anatomy and interpretation of the musculoskeletal system. *World Health Organization*; 2002:74

22. Subhawong TK, Fishman EK, Swart JE, et al. **Soft-tissue masses and masslike conditions: what does CT add to diagnosis and management?.** *AJR Am J Roentgenol* 2010;194:1559–67

23. Landis JR, Koch GG. **The measurement of observer agreement for categorical data.** *Biometrics* 1977;33:159–74

24. Koo TK, Li MY. **A Guideline of Selecting and Reporting Intraclass Correlation Coefficients for Reliability Research** *J Chiropr Med* 2016;15:155–63

25. Hosmer DW, Lemeshow S. **Applied Logistic Regression**, *John Wiley and Sons*; 2000:160–4

26. Milgram JW. **Synovial osteochondromatosis: a histopathological study of thirty cases.** *J Bone Joint Surg Am* 1977;59:792–801

27. Kendell SD, Collins MS, Adkins MC, et al. **Radiographic differentiation of enchondroma from low-grade chondrosarcoma in the fibula.** *Skeletal Radiol* 2004;33:458–66

28. Walker EA, Murphey MD, Fetsch JF. **Imaging characteristics of tenosynovial and bursal chondromatosis.** Skeletal Radiol 2011;40:317–25

29. Chen YX, Lu YX, Zhuang ZE, et al. **Extra-articular tenosynovial chondromatosis of the left ring finger in a 23-year-old man: A case report and literature review.** Exp Ther Med 2015;10:1581–3

30. Edeiken J, Edeiken BS, Ayala AG, et al. **Giant solitary synovial chondromatosis.** *Skeletal Radiol* 1994;23:23–9

31. Aoki J, Sone S, Fujioka F, et al. **MR of enchondroma and chondrosarcoma: rings and arcs of Gd-DTPA enhancement.** *J Comput Assist Tomogr* 1991;15:1011–6

32. Geirnaerdt MJ, Bloem JL, Eulderink F, et al. **Cartilaginous tumors:**

correlation of gadolinium-enhanced MR imaging and histopathologic findings. *Radiology* 1993;186:813–7

33. Sato J, Notani KI, Goto J, et al. **Synovial chondromatosis of the temporomandibular joint accompanied by loose bodies in both the superior and inferior joint compartments: case report**. *Int J Oral Maxillofac Surg* 2010;39:86–8

34. Chen MJ, Yang C, Cai XY, et al. **Synovial chondromatosis in the inferior compartment of the temporomandibular joint: different stages with different treatments.** *J Oral Maxillofac Surg* 2012;70:e32–8

35. Geirnaerdt MJ, Hermans J, Bloem JL, et al. **Usefulness of radiography in differentiating enchondroma from central grade 1 chondrosarcoma.** *AJR Am J Roentgenol* 1997;169:1097–104

36. Cawte TG, Steiner GC, Beltran J, et al. **Chondrosarcoma of the short tubular bones of the hands and feet.** *Skeletal Radiol* 1998;27:625–32

37. Murphey MD, Flemming DJ, Boyea SR, et al. **Enchondroma versus chondrosarcoma in the appendicular skeleton: differentiating features.** *Radiographics* 1998;18:1213–45

38. Fayad LM, Ahlawat S, Khan MS, et al. **Chondrosarcomas of the hands and feet: A case series and systematic review of the literature.** *Eur J Radiol* 2015;84:2004–12

국문 초록

CT와 MR 영상을 이용한 측두하악관절 연골육종과 활액연골종증의 감별

장 봉 근

서울대학교 대학원 치의과학과 영상치의학 전공

(지도교수 허 경 회)

1. 목적

활액연골종증과 연골육종은 측두하악관절에서 발생하고, 병소 내부에 연골성 석회화를 만들며, 하악 과두 및 관절융기 및 관절와에 골변화를 일으키는 대표적인 질환이다. 두 질환의 치료 계획이 서로 다르기 때문에, 두 질환을 감별하는 것이 매우 중요하지만 임상, 영상, 병리적으로 감별에 어려움이 있다. 이에 본 연구에서는 두 질환을 감별 할 수 있는 정성적 및 정량적 영상

소견을 찾아 그 감별진단능을 조사해보고자 하였다.

2. 재료 및 방법

2001-2020년에 서울대학교치과병원에 내원한 환자 중 연골육종과 활액연골종증으로 조직학적으로 진단된 환자 12명 및 35명의 CT, MR 영상 및 의무기록을 수집하였다. 두 명의 영상치의학 전문의가 병소 중심, 하악 과두 골파괴, 하악 과두 골경화, 관절융기/관절와 골파괴, 관절융기/관절와 골경화, 외측 익돌근의 익돌근와 부착 소실, 석회화 유무, 석회화 유형, 골막반응, 골극, 주변부 조영 증강, 내부 조영 증강, 그리고 병소 크기를 각각 평가하였다.

조사자간 일치도는 Cohen kappa 계수 및 intraclass correlation 계수를 구함으로써 평가하였다.

'High-risk clinical or imaging features'는 Fisher's exact test, chi-square test, linear-by-linear association test, Student's t-test, 및 receiver operating characteristic (ROC) analysis를 통해 통계적으로 활액연골종증보다 연골육종에서 더 자주 관찰되는 특징으로 정의되었다. 첫 단계로, 두 질환에 대한

변수의 통계적 유의성 분석에 Fisher's exact test, chi-square test, linear-by-linear association test, Student's t-test를 시행하였다. 두 번째 단계에서는 첫 번째 단계에서 유의미한 차이를 보인 변수에 대해, ROC 분석 및 Youden index 값을 구함으로써 두 질환을 감별해주는 cut-off 값을 구했다. 첫 번째 단계에서 유의미한 차이를 보인 변수에 대해, cut-off 값을 적용시켜, 'High-risk clinical or imaging features'를 결정하였다. 개별 'High-risk clinical or imaging features'의 CS에 대한 진단능을 알기 위해, sensitivity, specificity, accuracy, positive predictive value (PPV), negative predictive value (NPV), 및 area under the ROC curve (AUC)를 계산하였다. 또한 cut-off 값을 기준으로, 연골육종에 해당하는 소견의 경우 +1점을 부여하고, 활액연골종증에 해당하는 소견의 경우 0점을 부여하였다. 부여된 점수를 합하여 득점체계를 만들고, 그 진단능을 평가하였다.

3. 결과

Fisher's exact test, chi-square test, linear-by-linear association test, 및 Student's t-test에 의해 두 질환 간 유의한

차이를 보인 변수는 임상소견 변수들에서는 관찰되지 않았고, 영상소견 변수들에서만 관찰되었고, 다음과 같다: 1) 병소 중심, 2) 하악 과두 골파괴, 3)관절융기/관절와 골파괴, 4) 관절융기/관절와 골경화, 5) 외측 익돌근 부착 소실, 6) 석회화 유형, 7) 골막반응, 8) 내부 조영 증강, 9) 병소 크기.

ROC 분석을 통해 알게 된, 연골육종을 활액연골종증과 구별해주는 9 가지 영상 소견 각각의 cut-off 값은 다음과 같다: 1) 하악과두를 중심으로 함, 2) 하악 과두 골파괴의 존재, 3) 관절융기/관절와 골파괴의 부재, 4) 관절융기/관절와 골경화의 부재, 5) 외측 익돌근 부착 소실, 6) Stippled calcification, 7) 골막반응의 존재, 8) 내부 조영 증강의 존재, 9) 30.5 mm의 병소 크기

연골육종을 나타내는 'High-risk imaging features'로는 다음과 같다: 1) 하악 과두를 중심으로 함, 2) 하악 과두 골파괴의 존재, 3) 관절융기/관절와 골파괴의 부재, 4) 관절융기/관절와 골경화의 부재, 5) 외측 익돌근 부착 소실, 6) stippled calcification 혹은 석회화의 부재, 7) 골막반응의 존재, 8) 내부 조영 증강의 존재, 9) 30.5 mm 이상의 병소 크기

연골육종을 구별하기 위한 각각의 영상소견 변수들의 진단능 분석 결과, 최대 민감도 (100%)는 외측 익돌근 부착 소실 및 내부 조영 증강의 존재에서 관찰되었고, 반면 최대 특이도 (100%)는 하악 과두 중심에서 관찰되었다. 가장 뛰어난 AUC 값은 외측 익돌근 부착 소실에서 관찰되었다 (AUC=0.929 [95% CI, 0.855-1.000]). 연골육종을 구별하기 위한 9-scale composite scoring model의 진단능 분석 결과, best cut-off 값은 +4점이고 area under the curve 값은 0.958 [95% CI, 0.864-1.000]였다.

4. 결론

본 연구에서는 연골육종 및 활액연골종증의 감별에 있어 CT 및 MRI에서 관찰되는 영상 특징들이 탁월한 감별진단능(AUC = 0.958 [95% CI, 0.864-1.000])을 보여줄 수 있음을 확인하였다.

주요어: 연골육종, 활액연골종증, 측두하악관절, 감별 진단, 영상 특징

학 번: 2018-37587